

Not to appear in Nonlearned J., 45.

Total linear polarization in the OH maser W75N: VLBA polarization structure.

V. I. Slysh

*Astro Space Center, Lebedev Physical Institute, Profsoyuznaya 84/32, 117810 Moscow,
Russia*

vslysh@asc.rssi.ru

V. Migenes

*University of Guanajuato, Department of Astronomy, Apdo Postal 144, Guanajuato, CP
36000, GTO Mexico*

I. E. Val'tts

*Astro Space Center, Lebedev Physical Institute, Profsoyuznaya 84/32, 117810 Moscow,
Russia*

S. Yu. Lyubchenko

*Astro Space Center, Lebedev Physical Institute, Profsoyuznaya 84/32, 117810 Moscow,
Russia*

S. Horiuchi

*Astro Space Center, Lebedev Physical Institute, Profsoyuznaya 84/32, 117810 Moscow,
Russia*

V. I. Altunin

Jet Propulsion Laboratory, 4800 Oak Grove Dr., Pasadena, CA 91109, USA

E. B. Fomalont

National Radio Astronomy Observatory, 520 Edgemont Rd., Charlottesville, VA22903, USA

and

M. Inoue

Nobeyama Radio Observatory, Nobeyama, Minamisaku, Nagano 384-13, Japan

ABSTRACT

W75N is a star-forming region containing various ultracompact HII regions and OH, H₂O, and CH₃OH maser emission. Our VLBA map shows that the OH masers are located in a thin disk rotating around an O-star which is the exciting star of the ultracompact HII region VLA1. A separate set of maser spots is connected with the ultracompact HII region VLA2. The radial velocity of OH maser spots varies across the disk from 3.7 km s⁻¹ to 10.9 km s⁻¹. The diameter of the disk is 4000 A.U. All maser spots are strongly polarized. This are the first OH masers showing nearly 100 per cent linear polarization in several spots. Two maser spots seem to be Zeeman pairs corresponding to a magnetic field of 5.2 mgauss and 7.7 mgauss, and in one case we tentatively found a Zeeman pair consisting of two linearly polarized components. The linearly polarized maser spots are shown to be σ -components which is the case of the magnetic field being perpendicular to the line of sight. The direction of the magnetic field as determined from linearly polarized spots is perpendicular to the plane of the disk, although the galactic Faraday rotation may significantly affect this conclusion.

Subject headings: ISM: radio lines: ISM – masers – surveys – ISM: molecules

1. Introduction

OH maser emission is strongly polarized, usually in a circular mode, although an admixture of linear polarization was found in some masers, which resulted in the elliptical polarization mode. The importance of the polarization properties of OH masers lies in the physics of the maser excitation and saturation properties. Current theories of OH maser emission polarization attribute it to the magnetic field in the emission region, of the order of several milligauss. This is three orders of magnitude larger than the general galactic magnetic field, but is consistent with estimates of the maser emission region density of 10^6 – 10^7 cm⁻³ as originating from the compression of the interstellar matter and magnetic field. Determination of the magnitude and direction of the magnetic field will help to better understand the role of the magnetic field in the formation of circumstellar disks or shocks at the interface between compact HII regions and the ambient molecular cloud.

The polarization properties of OH maser emission were predicted by theoretical models on the basis of Zeeman splitting (Goldreich, Keeley, and Kwan 1973). If the Zeeman splitting

exceeds the line width ($B > 0.5$ milligauss), three 100 per cent polarized components are predicted: unshifted π -component linearly polarized along the projected direction of the magnetic field, and two 100 per cent elliptically polarized σ -components shifted in frequency to both sides of the π -component. The relative intensity of the π -component and the degree of ellipticity depend on the angle θ between the line of sight and the magnetic field direction. If $\theta = \pi/2$, the π -component is at maximum, and σ -components are linearly polarized perpendicular to the magnetic field direction. When $\theta = 0$, the intensity of the π -component is zero, and σ -components are 100 per cent circularly polarized in opposite directions. When $0 < \theta < \pi/2$, the π -component is linearly polarized along the magnetic field direction and is of intermediate intensity, and σ -components are elliptically polarized, with the major axis of the ellipsis perpendicular to the magnetic field. Such a picture has never been observed in OH masers in full details. Typically, individual maser spots were found to be highly circularly polarized only in one sense. In some cases opposite circular polarization was found to come from the same maser spot and was interpreted as a Zeeman pair. Linear polarization was rarely observed, and usually was found as part of the elliptically polarized emission. The best-studied region of OH maser polarized emission is W3(OH). Garcia-Barreto et al. (1988) found several dozens of circularly polarized components, with 16 being elliptically polarized. Only three components had linear polarization greater than circular polarization, with a maximum fractional linear polarization of 46 per cent. Five Zeeman pairs were identified. Garcia-Barreto et al. (1988) came to the conclusion that no features were detected that might have been identified as π -components. Most of the details were single, circularly polarized features. In a similar polarization study of G35.02–0.74N with a lower angular resolution Hutawarakorn and Cohen (1999) found 25 circularly polarized spectral features, with four Zeeman pairs and five features in which linear polarization was also present, with a maximum fractional polarization of 63 per cent. They were considered as σ -components.

W75N is another well-studied OH maser source. It is associated with a star-forming region and an ultracompact HII-region, at a distance 2 kpc (Habing et al. 1974). VLBI maps of the OH main line, 1665 MHz, show nine components in the elongated region 1.5" in extent (Haschick et al. 1981). From a single antenna polarization study Haschick et al. (1981) were able to determine polarization of some maser spots in their VLBI map, and suggested two Zeeman pairs with opposite circular polarization. A true high angular resolution polarization study of W75N was conducted with MERLIN by Baart et al. (1986). They also found several Zeeman pairs of oppositely circularly polarized spectral features coming from the same position within measurement errors. In addition they suggested that there may be seven linearly polarized components present. This suggestion was based on the presence of opposite circularly polarized pairs of spectral features coming from the same position and having the same radial velocity, in contrast with Zeeman pairs having different

radial velocities. No cross-correlation measurements were done in this study, which are needed to measure linear polarization.

The prevalence of circular polarization and a scarcity of linear polarization is a long standing problem in maser polarization theory. Goldreich, Keeley, and Kwan (1973) have proposed that the Faraday rotation in the emission region might destroy linear polarization, and only circular polarization remains. If the linear polarization suggested by Baart et al. (1986) is real, it might be used for testing polarization models. The polarization structure of OH masers may be smeared by the lack of spectral and angular resolution when several adjacent features are mixed. Baart et al. (1986) made their study with the angular resolution of 280 mas and spectral resolution of 0.3 km s^{-1} , which is insufficient as will be seen from our results.

In this paper we present a new polarization study of W75N with much higher angular and spectral resolution, and with a full polarization analysis making use of all Stokes parameters. This made it possible to exclude any contamination of spectral features by a contribution from other spectral features. In addition, for the first time, polarization mapping of W75N in another main line OH transition, 1667 MHz, has been performed.

2. Observations and data reduction

The observations were made on 1998 July 1 as a part of the survey of compact OH masers suitable for further observations with the space ground interferometer (Migenes et al. 2001). We used the VLBA in a snap-shot mode, observing every source with a 5 minute scan. The synthesized beam of the array at the OH frequency, 1665/1667 MHz, was elliptical, 12×4 mas with the position angle of the major axis -5° , which corresponds to the size and orientation of the VLBA at the moment of the snap-shot observation. The observations were carried out at all four OH line frequencies, in two circular polarizations, with the bandwidth of 125 kHz (25 km s^{-1}) divided in 128 spectral channels at each OH frequency which provided a spectral resolution of 0.176 km s^{-1} . The correlation was done with the NRAO VLBA correlator in Socorro in the full cross-correlation mode providing four correlated complex spectra RR, LL, RL and LR for each pair of antennas. These outputs can be used for determination of Stokes parameters in a standard way:

$$\begin{aligned} I &= \frac{1}{2}(RR + LL) & V &= \frac{1}{2}(RR - LL) \\ Q &= \frac{1}{2}(RL + LR) & U &= \frac{i}{2}(LR - RL) \end{aligned} \quad (1)$$

The amplitude calibration was performed using the system noise temperature and gain curves provided by VLBA Operations. Continuum sources 3C273 and OQ208 were used for the band pass and polarization calibration. Fig. 1a,b show images of 3C273 and OQ208 in I (contours) and linearly polarized intensity (vectors). The vectors shown in Fig. 1a correspond to a fractional linear polarization $m_L=1.4$ per cent; the circular polarization measured on 3C273 is $m_C=1.8$ per cent. No calibration of the position angle of the linear polarization has been done. In principle, one could calibrate the position angle by rotating the measured linear polarization vector of 3C273 to the published value (e.g. (Conway et al. 1993)) and applying this correction to W75N OH maser data. However, we considered this to be of little usefulness because observations of W75N have been performed 7.5 hours after observations of 3C273, and during that time interval ionospheric Faraday rotation could change significantly direction of the polarization vector. Moreover, in view of the uncertain correction for the Galactic Faraday rotation (Section 4.2) the absolute position angle of the linear polarization remains unknown, and in what follows we give only relative position angles which are rotated by an unknown amount. For OQ 208 linear polarization vectors correspond to $m_L \leq 0.1$ per cent they are distributed over the entire field and are caused by noise; the circular polarization is also $m_C=1.8$ per cent. OQ208 is known to be unpolarized (Stanghellini et al. 1998), while the 18 cm linear polarization of the core of 3C273 shown on Fig 1a is $m_L=1.8 - 2.15$ per cent (Conway et al. 1993), which is close to our result on Fig. 1a taking into account the crudeness of the snap-shot measurements. In any case it would be safe to disregard any linear polarization below 1 per cent. As for the circular polarization which is known to be absent in these two sources, the consistency of the two measurements means that there is unaccounted instrumental polarization in a sense that the intensity of the right circular polarization is systematically larger than the intensity of the left circular polarization. In presenting the OH maser data we made a correction for the instrumental polarization by subtracting 1.8 per cent from all fractional polarization values of m_C . These corrections are small compared to the fractional polarization measured for OH spectral features.

The calibration was performed by the self-calibration of the reference spectral feature using AIPS task "FRING". The reference feature was chosen such as to allow calibration of both RCP and LCP channels of the receiver. This is possible if a spectral feature emits strongly enough in both modes of polarization from the same position. To satisfy these requirements the feature must be either unpolarized, or linearly polarized. Since for OH masers unpolarized features are rare, we looked for linearly polarized features. Fig. 2 (upper) shows the cross-polarized spectrum RL on the baseline Kitt Peak – Pie Town. The non-zero features in this cross-polarization spectrum (i.e. a correlated spectrum from a pair of antennas with opposite circular polarizations) are due to the linear polarization. There

are several linearly polarized features in the spectrum which can be taken as a reference. We took the feature at 5.65 km s^{-1} which showed the largest correlated flux on the longest baseline, Mauna Kea – Saint Croix, and could be used for calibrating all the antennas of the array.

The calibration of the array was performed by means of fringe fitting to the reference feature. A correction to the position of the phase center adopted at the correlator was made using the measured absolute position of the reference feature. The absolute position was measured by the fringe rate method. Since the position offset of different spectral features in W75N is known to be quite large compared to the size of the map, the mapping was carried out in two steps. First, an approximate position of all spectral features relative to the reference feature was determined with the fringe rate method. Then maps of spectral features were constructed centered on these approximate positions. From the maps relative positions and angular dimensions were determined by fitting two-dimensional Gaussians and deconvolving them with the beam. Separate maps of spectral features were obtained in all Stokes parameters: I, Q, U and V. From the first three Stokes parameters polarization maps were constructed, which show total intensity I contours and linear polarization vectors.

The 1667 MHz data were considered as independent from the 1665 MHz data and were calibrated separately, using the feature at the radial velocity of 9.8 km s^{-1} (Fig. 2 lower) as a reference. The absolute position of the 1667 MHz reference feature was determined by the fringe rate method independently from the 1665 MHz measurements, with a lower accuracy than the relative position measurement accuracy.

3. Results

3.1. Spectrum

The cross-correlated circularly polarized spectra of the 1665 MHz line are shown in Fig. 3. If compared with spectra taken in 1975 by Davies et al. (1977) one can see many changes. The strongest component is the RCP feature near 12 km s^{-1} with the same flux density, but with the radial velocity shifted to 12.45 km s^{-1} . A nearby weaker component at 13 km s^{-1} has disappeared since 1975. Two new RCP features have appeared, at 0.65 km s^{-1} and 3.0 km s^{-1} . In the LCP spectrum a new component at 9.4 km s^{-1} has appeared, as well as a component at 0.65 km s^{-1} . The 1667 MHz spectrum shows less spectral features, and they occupy a smaller velocity range. The total intensity cross-correlated spectra at 1665 MHz and 1667 MHz are shown in Fig. 4a,b. There seems to be no one-to-one correspondence between the spectral features in the two main OH lines. No emission features were found in

the OH satellite lines at 1612 MHz and 1720 MHz.

3.2. Absolute position

The absolute position of the 1665 MHz reference feature is given in the footnote to Table 1. It is a factor of 3 more accurate than the previously measured absolute position (Haschick et al. 1981), but both measurements give coinciding positions within the combined error box. The absolute position of the strongest 1667 MHz feature at 9.8 km s^{-1} was measured independently, and was found to be shifted in the sky from the 1665 MHz reference feature by -175 ± 69 mas in right ascension (offsets in right ascension mean R.A. $\times \cos(\text{Dec})$) and by -661 ± 42 mas in declination.

3.3. Distribution of maser spots

Eleven maser spots were identified at the 1665 MHz transition and four at the 1667 MHz. In Table 1 we present the relevant parameters for the maser spots determined from their spectra and from polarization maps: LSR radial velocity, Stokes parameters (I, V, Q, U), percentage of circular (m_C) and linear (m_L) polarization, linear polarization position angle χ , offsets in R.A. and Dec. from the reference position, deconvolved angular dimensions of the fitted elliptical Gaussians and their position angle Θ . The error in the relative positions is less than 1 mas. The position error of the 1667 MHz spot L is much larger since it was determined by fringe rate method, but the position errors of the rest of the 1667 MHz spots relative to spot L is less than 1 mas. The position of the maser spots is shown on Fig. 5. Also shown are the ultracompact HII regions VLA1 and VLA2 (Torrelles et al. 1997). Most of the spots lie on an almost straight line of $1.6''$ (3200 A.U.) in extent, slightly displaced from VLA1. The 1667 MHz spots do not coincide with any of 1665 MHz spots, however they are located in the same general area. The radial velocity varies along the line from 3.8 km s^{-1} to 10.9 km s^{-1} (this is the mean radial velocity of features A and B, which come from the same position as a Zeeman pair), moving from North to South. Two separate spots, J and K are located near the second ultracompact HII region VLA2. The map closely resembles the MERLIN map by Baart et al. (1986). All our 1665 MHz spots can be found on the Baart et al. (1986) map, except for spot K at 0.65 km s^{-1} . There are several weak spots on the MERLIN map which are not present on our map but this can be due to our poorer sensitivity. The 1667 MHz map has been built for the first time, and no comparison with earlier maps is possible. Also, a good correspondence is found with the VLBI map by Haschick et al. (1981). The only significant difference between our map and those of Baart et al. (1986)

and Haschick et al. (1981) is the shifted position of spot A (12.45 km s^{-1}) by 140 mas; note, that the radial velocity of this feature has also changed by 0.45 km s^{-1} . One can not be sure that feature A is identical to the 12 km s^{-1} feature in earlier maps, it is possible that the 12 km s^{-1} feature has disappeared, and that feature A is a new feature which has flared up not far from the 12 km s^{-1} position. On the other hand the identification of feature A with the 12 km s^{-1} feature is supported by its dominance in both spectra and by the equality of flux densities.

3.4. Spot size and brightness temperature

All maser spots have been partially resolved. From Table 1 one can see that the largest spots are spot K ($20 \text{ mas} \times 12 \text{ mas}$) and spot N ($14 \text{ mas} \times 3 \text{ mas}$), but they may consist of several smaller spots which we can not resolve. The rest of the spots can be fitted with Gaussians with the major axis from 4.4 to 10.7 mas, and the minor axis from 0.7 to 4.6 mas. Considering that the beam size is 12×4 mas, 0.7 mas must be regarded only as a formal fitting solution. The real extent of the minor axis can be much less than the indicated, so it should be considered as an upper limit. The brightness temperature of one of the brightest 1665 MHz spots, F (reference feature), with the integrated flux density of 18.1 Jy is $1.6 \times 10^{12} \text{ K}$. The brightest 1667 MHz spot is L, with the integrated flux density 31.9 Jy, and it has a brightness temperature of $1.9 \times 10^{12} \text{ K}$. These must be regarded as lower limits since most of the spots are probably not resolved along the minor axis. All the mapped spots are elongated, with the major to minor axis ratio 3 or higher. If the size of the maser spots is not intrinsic and is caused by the scattering in the interstellar medium, then the elongation of the spots may be a result of the anisotropic scattering.

3.5. Polarization of maser spots

All maser spots given in Table 1 were imaged in all Stokes parameters. This made it possible to determine full polarization properties of the maser spots. The percentage of circular polarization given in Table 1 was calculated as

$$m_C = 100 \frac{V}{I} \quad (2)$$

Positive V corresponds to the right circular polarization. Percentage of the linear polarization was calculated as:

$$m_L = 100 \frac{\sqrt{Q^2 + U^2}}{I} \quad (3)$$

and the position angle of the electric vector of linear polarization was calculated as

$$\chi = \frac{1}{2} \arctan \frac{U}{Q} \quad (4)$$

with positive direction East of North. I , Q , U , V are Stokes parameters at the maximum of the corresponding spot maps (Jy/beam). In some cases the percentage of the polarization exceeds 100. This may be due to a difference in the position of maxima in different Stokes parameters, as well as to errors of intensity measurements.

From Table 1 it is evident that the maser spots are highly polarized, typically 100 per cent polarized. There are 2 types of the maser spots. The first type is strongly linearly polarized spots with $m_L > 70$ per cent (E,F,G,H,J,K). Polarization of the spots in this group is not purely linear, it has an admixture of small circular polarization, making the polarization elliptical. The percentage of circular polarization varies from less than 0.3 per cent to 80 per cent. Baart et al. (1986) suggested several candidates as linearly polarized components, based on the small difference in position and equal velocities of several oppositely circularly polarized pairs. Now, with the full polarization analysis and a much higher position accuracy we can confirm or reject Baart et al. (1986) candidates. We confirm five of seven MERLIN candidates: J=A,A; G=F,C; F=G,D; E=H,E; A,B=N,K. The former is the spot designation in Table 1, and the latter are designations by Baart et al. (1986). Two other candidates, D,B and M,J were not present in our data. The spot A,B=N,K is predominantly circularly polarized, with linear polarization of only 9.3 per cent. There is a pair of oppositely polarized spectral features at the radial velocity 9.35 km s^{-1} , which looks like a linearly polarized feature suitable for the calibration; but it is absent in the cross-polarized spectrum in Fig.2a which means that the left-hand and right-hand polarized emission come from different positions, which has been confirmed by the subsequent mapping (features B and C in table 1). This is a chance coincidence of radial velocities of two independent maser spots with opposite circular polarization which could be mixed with linear polarization in the absence of the full polarization analysis and high angular resolution mapping. In the 1667 MHz transition there is only one linearly polarized spot, with a percentage of linear polarization of 41.6 per cent, and with a circular polarization fraction of 23 per cent.

The position angle of the linear polarization vector is in the range of -23° to 23° for the spots in this group. The mean position angle of the linear polarization vector is $3.9^\circ \pm 17^\circ$ (Fig. 6). Fig. 7 shows polarized and total intensity images of several linearly polarized spots.

The other type of maser spots is strongly circularly polarized, with an admixture of

linear polarization (spots A–D,I,M,N,O). The percentage of the circular polarization in this group is close to 100 per cent, and the fractional linear polarization is of less than 5 per cent to 17.9 per cent, and only spot L has moderate linear and circular polarization.

3.6. Identification of Zeeman pairs

The 1665 MHZ emission from spots A and B, and from spots M and O at 1667 MHz come from the same positions, with the position difference 0.8 mas and 1.1 mas, respectively, which is much less than the size of the beam and the size of the spots. The polarization is oppositely circular, and the velocity difference is 3.07 km s^{-1} and 2.7 km s^{-1} , respectively. Based on these properties one can identify these two pairs as $\sigma\pm$ -components of the Zeeman pattern, with the magnetic field 5.2 mgauss and 7.7 mgauss, respectively (positive sign indicates field direction pointing away from the Earth). Both pairs are elliptically polarized, with nearly the same position angles of the polarization vector, exactly as required for σ -components. Nevertheless there are distinctions from the theoretical Zeeman pattern. The first is the inequality of the intensities of right-hand and left-hand polarized emission. The intensity ratio of circularly polarized components is 5 for the A,B pair, and 1.8 for the M,O pair. Linearly polarized intensities are also different, the ratio being 2.2 for the A,B pair and 1.2 for the M,O pair. Another important deviation from the theoretical Zeeman pattern is the complete absence of π -components. In a Zeeman pair the π -component must be located at the mean radial velocity of the pair. We conducted an intense search for π -components for the two Zeeman pairs: A,B at the radial velocity of 10.9 km s^{-1} and for M,O at the radial velocity of 7.3 km s^{-1} , and did not find any emission above the noise level. Also, a π -component must be only linearly polarized, and we found that every maser spot is elliptically polarized. The only spot for which the circular polarization was not detected is spot E. Therefore we conclude that π -components are not present in the Zeeman spectrum of OH masers in W75N. Baart et al. (1986) suggested several Zeeman pairs, none of which are confirmed here. For the pair with radial velocities of 3.8 km s^{-1} (LCP) and 6.5 km s^{-1} (RCP) suggested by Baart et al. (1986) we confirm only the LCP-component, with LCP/RCP ratio above 28; the LCP/RCP ratio in Baart et al. (1986) is 5. In addition, for the other Zeeman pair suggested by Baart et al. (1986) with radial velocity of 4.8 km s^{-1} (LCP) and 9.6 km s^{-1} (RCP) we could not find the LCP counterpart, with the RCP/LCP ratio of more than 350 while Baart et al. (1986) data suggest RCP/LCP=12.

Haschick et al. (1981) suggested two possible Zeeman pairs which are not present in our data. The discrepancy between our data and earlier results can be attributed to the the variability of the Zeeman component intensity. We never see equal intensity of σ –

components, and the intensity ratio can vary in a very large range. If the σ -component intensity ratio is very large, the weaker component becomes unobservable. This may explain the presence of single circularly polarized spectral features in OH masers.

3.7. Polarization status

On Fig. 8 we show the percentage of circular polarization plotted against the percentage of linear polarization for all spots. The spots are labelled by letters as in Table 1. The dashed line shows where completely polarized features could appear on the diagram. The majority of the spots are located close to the 100 per cent polarization line. A notable exception is spot L (1667 MHz transition) which is 47 per cent polarized. There is evidence for a correlation in that predominantly circularly polarized spots are either located in the upper and lower left corners of the diagram, and predominantly linearly polarized spots are located in the middle right of the diagram. The numbers on the dashed line indicate an angle θ between the line of sight and the magnetic field direction, according to equations

$$m_L = 100 \frac{\sin^2 \theta}{1 + \cos^2 \theta} \quad m_C = \pm 100 \frac{\cos \theta}{1 + \cos^2 \theta} \quad (5)$$

These equations describe polarization of the σ -components in the theory by Goldreich, Keeley, and Kwan (1973) for the case when the Zeeman splitting is larger than the linewidth (see also Elitzur 1996). Most of the maser spots occupy two regions on the diagram: $\theta < 30^\circ$ and $80^\circ < \theta < 90^\circ$. If all the spots are σ -components it means that the line of sight is either parallel or perpendicular to the magnetic field direction, and no intermediate cases exist. The predominantly circularly polarized spots are almost certainly σ -components, although frequently without the second member of the pair. The predominantly linearly polarized spots are also σ -components with $\theta \approx 90^\circ$, or π -components. A correct attribution is important for the determination of the direction of the magnetic field: it is parallel to E-vector for π -components, and perpendicular to E-vector for σ -components. As mentioned in Section 3.6 the presence of the small circular polarization makes these components elliptically polarized, and therefore they must be σ -components, since π -components can not have a circular polarization contribution.

The only linearly polarized spot, L at 1667 MHz, is definitely not 100 per cent polarized and is an exception among all maser spots in W75N. In the model of the weak magnetic field the percentage of linear polarization for $\sin^2 \theta > 1/3$ is

$$m_L = 100 \frac{3 \sin^2 \theta - 2}{3 \sin^2 \theta} \quad (6)$$

(Goldreich, Keeley, and Kwan 1973). For this spot $m_L = 41.6$ per cent, and corresponds to $\theta = 43.4^\circ$. The percentage of circular polarization varies across the line profile (Fig. 9) changing the sign as predicted by the theory for the case of small Zeeman splitting (Elitzur 1996). However the curve is shifted from the line centre and is strongly distorted compared to the theoretical one, probably because of the non-linear mode competition in the maser. The linear polarization increases to the red-side of the profile, while the circular polarization is larger at the blue side.

4. Discussion

4.1. Linear polarization

The most important result of this study is the discovery of several linearly polarized maser spots with almost 100 per cent polarization. The mere existence of linear polarization in these spots and in the circularly polarized spots means that the Faraday rotation proposed by Goldreich, Keeley, and Kwan (1973) as a mechanism for the elimination of π -components is not important in W75N OH maser. The linearly polarized components are σ -components of the Zeeman pattern. This conclusion can be tested if the second σ -component of the Zeeman pair of linearly polarized emission will be found, shifted in radial velocity by an appropriate amount. We tentatively found the Zeeman counterpart F1 to the linearly polarized feature F. It is shifted in the radial velocity by 6.3 km s^{-1} , corresponding to the magnetic field strength 10.7 milligauss, and is almost fully linearly polarized, with the position angle close to the position angle of spot F. This is consistent with the σ -component interpretation of spots F and F1. However, this conclusion has to be confirmed with a more sensitive measurements, since the detection of the component F1 is tentative. Its intensity is only about 0.003 of intensity of component F, and it was detected on the edge of the spectral band of the receiver, in fact, in the last 128th channel. This is not surprising since the Zeeman pairs were found in W75N, with unequal intensity of the components. The linearly polarized Zeeman counterpart pairs might be too weak for a detection. The difference in intensity of Zeeman σ -components seems to be a widespread property of OH masers, and is probably due to a gradient of the radial velocity and magnetic field (Cook 1966). The absence of π -component is more difficult to understand. As mentioned above internal Faraday rotation can not be responsible for this. Maser model calculation by Gray and Field (1995) produce both π and σ -components, with σ -components dominating over π -components in the range of angles

$\theta = 0 - 55^\circ$, where σ -components are circularly or elliptically polarized. For $\theta = 55 - 90^\circ$, π -components which are linearly polarized dominate. Saturation effects of competitive gain strongly reduce a weaker component, that is π -component for $\theta = 0 - 55^\circ$, and σ -component for $\theta = 55 - 90^\circ$. Gray and Field (1995) note that the suppression of σ -component is much less efficient, than the suppression of π by σ -components. The model of Gray and Field (1995) is in conflict with our conclusion that linearly polarized spots in W75N are emitting σ -components with θ close to 90° , while the model predicts dominance of the linearly polarized π -components for θ near 90° . Our identification of the linearly polarized spots as σ -components was based on the presence of some circularly polarized emission in all spots except spot E. This seems to be a very firm argument in favor of σ -components unless an explanation for the circular polarization contribution to the π -components is found.

There is an alternative interpretation of the observed linear polarization as a result of the saturated maser amplification with a weak magnetic field, when the Zeeman splitting is less than the bandwidth. For $\sin^2 \theta \leq 1/3$, or $\theta \leq 35.5^\circ$ there will be a single 100 per cent linearly polarized emission line with E-vector parallel to the magnetic field direction (Case 2a in Goldreich, Keeley, and Kwan (1973)). For $\theta > 35.5^\circ$ the linear polarization will be lower, and the circular polarization appears in the line wings (see Section 3.7). This model could explain observed linearly polarized emission in W75N but the observed admixture of circular polarization remains unaccounted, the same as for the π -components in the Zeeman splitting. Also this model limits the magnetic field to about 0.5 milligauss which is much less than was deduced for spots A, B, F, F1 and M, O in Section 3.6. More likely this explanation could be applied to the observed linear polarization of H₂O and methanol masers. And, finally, the detection of the Zeeman counterpart F1 the spot F, if confirmed, is a definite proof of the interpretation of the linearly polarized emission features as σ -components of Zeeman pattern.

4.2. The nature of maser spots

We have mapped 14 maser spots in W75N (Fig. 5), with two or possibly three coinciding Zeeman components. Every maser spot has its own radial velocity, different from the radial velocity of other spots, and a narrow line width of about $0.2 - 0.3 \text{ km s}^{-1}$. 1667-MHz spots do not coincide in position with 1665-MHz spots. Almost every spot is 100 per cent elliptically polarized. We interpret them as σ -components of the Zeeman pattern. The magnetic field in the Zeeman pairs was determined to be from 5 to 11 milligauss, the same values as found in other OH masers (Garcia-Barreto et al. 1988). One can assume that in other spots where the second σ -component is not visible the magnetic field strength is of the same order. If it

is a σ -component, then the linear polarization vector must be perpendicular to the direction of the magnetic field, and the magnetic field direction seems to be roughly the same for all spots. This can be seen on the histogram in Fig 6. Unfortunately the direction of the magnetic field can not be determined reliably from the linear polarization measurements because of the uncertain amount of Faraday rotation in the Galaxy. The OH masers are located in the Galactic disk where the Faraday rotation is at maximum. Total Faraday rotation in the Galactic plane as measured with extragalactic radio sources is

$$RM(l) = RM_0 \sin(l_0 - l) \quad (7)$$

where $RM_0 = 1607 \text{ rad m}^{-2} \pm 10$ per cent r.m.s., $l_0 = 62.1^\circ$ (Clegg et al. 1986). W75N is at the galactic longitude $l = 81.9^\circ$, and from (7) one has $RM = -544 \text{ rad m}^{-2}$. At the OH frequency ($\lambda = 18 \text{ cm}$) the Faraday rotation is $(-544) \times (0.18)^2 = -17.6 \text{ rad} \pm 5.4 \text{ rad}$ if one assumes maximum uncertainty 30 per cent. This is the total Faraday rotation throughout the galactic disk; W75N is at the distance of 2 kpc, which is probably about a half of the total effective distance, and the Faraday rotation to W75N can be a factor of 2 lower, or $-9 \text{ rad} \pm 2.7 \text{ rad}$. This is a large rotation, about 3 full turns, and a correction for the Faraday rotation to the position angle of the linear polarization could be quite uncertain. Therefore it is not possible to determine the direction of the magnetic field in OH maser spots.

Physical parameters of the maser spots can be estimated from maser models, which require gas density $n_{H_2} = 10^7 \text{ cm}^{-3}$, kinetic temperature 100 K, dust temperature 150 K, and OH abundance 10^{-5} (Gray and Field 1995). Such parameters can provide inversion of 1665 MHz OH transition in a model with FIR line overlap and a velocity gradient of about $0.025 \text{ km s}^{-1}/\text{A.U.}$ (Gray and Field 1995). With the magnetic field strength of 10 milligauss the model of Gray and Field (1995) provides 100 per cent elliptically polarized σ -components, with π -components suppressed, in agreement with results of this paper for W75N. The size of maser spots 10 A.U. and molecular hydrogen density 10^7 cm^{-3} correspond to the mass of maser spots of $2 \times 10^{-7} M_\odot$, which is less than the mass of the Earth.

If the maser spots are discrete physical objects – dense cold gas condensations surrounded a low density medium – they should be confined by the external pressure. A gas condensation with the density 10^7 cm^{-3} and temperature 100 K can be in pressure equilibrium with the gas of density 10^5 cm^{-3} and temperature 10^4 K . However, the magnetic pressure in the maser spots, with the magnetic field strength of 10 milligauss, is an order of magnitude higher, and can be compensated by turbulent or ram pressure of the hot medium (see discussion in a paper by Reid et al. (1987)). Another model of maser spots proposed for Class II methanol masers (Slysh et al. 1999) assumed that the maser spots are extended gaseous envelopes of solid icy planets orbiting around O, B-stars, outside their HII regions.

OH molecules as well as methanol molecules are continuously supplied to the envelope by evaporation of ice from the surface of the planets. In W75N the ultracompact HII region VLA1 (Fig. 5) marks the position of the central star with luminosity $1.4 \times 10^5 L_\odot$ (Moore et al. 1991) which corresponds to the main sequence O9-star with mass $20M_\odot$. The largest distance from VLA1 to a maser spot is about 1000 mas, or 2000 astronomical units. At this distance from a $20M_\odot$ star the orbital velocity is 3 km s^{-1} which is consistent with the observed velocity range of maser spots in W75N. In this model the magnetic field originates in the planets.

4.3. The model of region W75N

OH maser spots in W75N are located around the ultracompact HII region VLA1, with spots J and K possibly associated with another ultracompact HII region, VLA2 (Fig 5). One model of OH masers places them at D-type ionization front (Elitzur and de Jong 1978) or in the photo-dissociation region (Hartquist and Sternberg 1991) surrounding the HII-region. In W75N the geometry of OH maser spots is consistent with these models although the observed gradient of the radial velocity along the chain of maser spots from about 10 km s^{-1} at spots A, B to 3.7 km s^{-1} at spot I is not predicted by the models. This gradient is better represented in the model of jet or in disk models. Torrelles et al. (1997) based on the elongated shape of the ultracompact HII-region VLA1 and orientation of chains of H_2O and OH maser spots parallel to the direction of the bipolar outflow, observed in W75N on a much larger scale, suggested that the masers trace the outflow at scales of about 1 arcsec and that VLA1 is the powering source of the molecular outflow. Our more accurate measurements of the absolute position of OH masers show that they are not projected at VLA1 (Fig 7 in Torrelles et al. (1997)) but are displaced to form an arc around VLA1. The H_2O masers seem to form an arc which is closer to VLA1. Such a geometry is better described by a disk around VLA1 in which OH maser spots are located at a distance of about 2000 astronomical units from VLA1, and H_2O masers are located a factor of 2 to 5 closer. The disk model was first suggested by Haschick et al. (1981). VLA1 marks the position of the ionization source and the center of gravity of the system. As was suggested in Section 4.2 there might be a $20M_\odot$ O9-star at the center of VLA1, which gravitationally holds the disk of radius 2000 astronomical units. In this model the elongated shape of VLA1 reflects the distribution of disk material, which became visible in radio due to the ionization by the central star. We can not determine direction of the magnetic field in the disk from linear polarization data because of the uncertain amount of Galactic Faraday rotation (see Section 4.2) but we can state that the distribution of the magnetic field orientation is not random and is well organized in some direction, as is evident from the histogram of Fig 6.

5. Conclusions

- One of the results of this study is the discovery of several linearly polarized maser spots with almost 100 per cent polarization.
- For the first time polarization mapping of W75N in another main line OH transition, 1667 MHz was done.
- We suggest that the OH masers are located in a thin disk rotating around an O-star which is the exciting star of the ultracompact HII region VLA1. The diameter of the disk is 4000 A.U. Two separate maser spots are connected with the ultracompact HII region VLA2.
- Spots A and B at 1665 MHz and M and O at 1667 MHz come from the same positions. The polarization is oppositely circular, and the position difference is very small. Based on these properties one can identify these two pairs as $\sigma\pm$ -components of Zeeman pattern. Both pairs are elliptically polarized, with nearly the same position angles of the polarization vector, exactly as required for σ -components. Two maser spots show Zeeman pairs corresponding to the magnetic field 5.2 mgauss and 7.7 mgauss.
- The linearly polarized maser spots are shown to be σ -components in the case of the magnetic field perpendicular to the line of sight. We tentatively detected a Zeeman pair consisting of the linearly polarized components, with a deduced magnetic field of 10.7 mgauss. The direction of the magnetic field as determined for linearly polarized spots is perpendicular to the plane of the disk, not corrected for the Galactic Faraday rotation.

Acknowledgements

NRAO is a facility of the National Science Foundation operated under a cooperative agreement by Associated Universities. VIS and IEV acknowledge partial support from INTAS (grant N97-11451) and Russian Foundation for Basic Research (grant N01-02-16902).

REFERENCES

Baart, E. E., Cohen, R. J., Davies, R. D., Norris, R. P., and Rowland, P. R. 1986, MNRAS, 219, 145

Clegg, A. W., Cordes, J. M., Simonetti, J. K., and Kulkarni, S. R. 1992, ApJ, 386, 143

Conway, R. G., Garrington, S. T., Perley, R. A., and Biretta, J. A. 1993, *A&A*, 267, 347

Cook, A. H., 1966 *Nature*, 211, 503

Davies, R. D., Booth, R. S., and Perbet, J.-N. 1977, *MNRAS*, 181, 83

Elitzur, M. 1996, *ApJ*, 457, 415

Elitzur, M., and de Jong, T. 1978, *A&A*, 67, 323

Garcia-Barreto, J. A., Burke, B. F., Reid, M. J., Moran, J. M., Haschick, A. D., and Schilizzi, R. T. 1988, *ApJ*, 326, 954

Goldreich, P., Keeley, D. A., and Kwan, J. Y. 1973, *ApJ*, 179, 111

Gray, M. D., and Field, D. 1995, *A&A*, 298, 243

Habing, H. J., Goss, W. M., Matthews, H. E., and Winnberg, A. 1974, *A&A*, 35, 1

Hartquist, T. W., and Sternberg, A., 1991, *MNRAS*, 248, 48

Haschick, A. D., Reid, M. J., Burke, B. F., Moran, J. M., and Miller, G. 1981, *ApJ*, 244, 76

Hutawarakorn, B. and Cohen, R. J., 1999, *MNRAS*, 303, 845

Migenes, V., Slysh, V. I., Val'tts, I. E., Horiuchi, S., and Inoue, M. 2001, *ApJ*, (in preparation)

Moore, T. J. T., Mountain, G. M., and Yamashita, T. 1991, *MNRAS*, 248, 79

Reid, M. J., Myers, P. C., and Bieging, J. H. 1987, *ApJ*, 312, 830

Slysh, V. I., Val'tts, I. E., Kalensky, S. V., and Larionov, G. M. 1999, *Astronomy Report*, 43, 785

Stanghellini, C., Dallacasa, D., O'Dea, C. P., Baum, S. A., Fanti, C., and Fanti, R. 1998, *Proceedings of the IAU Colloquium 164*, eds. J. A. Zensus, G. B. Taylor, & J. M. Wrobel, *A.S.P. Conference Series*, p.177

Torrelles, J. M., Gomez, J. F., Rodriguez, L. F., Ho, P. T. P., Curiel, S., and Vazquez, R. 1997, *ApJ*, 489, 744

Table 1. Maser spots in W75N

Spot	v_{lsr} km s $^{-1}$	I Jy/beam	V Jy/beam	Q Jy/beam	U Jy/beam	m_C per cent	m_L per cent	χ °	$R.A.$ mas	$Dec.$ mas	Size mas	Θ °
1665 MHz												
A	12.45	16.88	16.24	<0.04	-1.56	94.4	9.3	-45.0	-301.7	-1176.7	5.9×1.4	95
B	9.38	3.92	-3.24	-0.17	-0.68	-84.4	17.9	-52.2	-301.1	-1177.3	5.5×4.6	86
C	9.35	3.27	3.50	0.11	-0.19	105.3	6.9	-29.8	-98.2	-573.5	5.6×4.1	61
D	7.35	0.61	0.62	<0.02	<0.02	101.2	<5.0	...	-1.0	-32.7	4.4×1.1	83
E	6.00	5.76	<0.02	4.71	2.69	<0.3	94.2	14.9	-122.7	-663.6	5.9×2.2	92
F *	5.65	10.16	-0.81	6.93	7.12	-9.8	97.8	22.9	0.0	0.0	5.4×1.2	96
G	5.29	3.30	-0.78	2.37	1.87	-25.4	91.4	19.2	155.5	114.2	7.6×2.9	59
H	5.11	2.86	-2.24	1.41	-1.45	-80.0	70.7	-22.9	186.9	167.1	5.1×2.5	94
I	3.70	1.18	-1.28	<0.02	0.13	-110.8	10.8	40.6	249.0	317.9	6.5×2.9	77
J	3.00	8.16	0.79	7.61	-3.05	7.9	100.5	-10.9	299.8	-1275.8	10.7×2.4	114
K	0.65	0.83	0.22	0.78	<0.009	24.2	93.7	0.0	376.5	-1385.3	19.7×11.9	142
F1	-0.65	0.040	< 0.003	0.035	0.023	< 10	87	20.5	0.14	0.47	6.5×0.7	74
1667 MHz												
L	9.80	21.33	-4.46	6.01	6.54	-22.7	41.6	23.7	-175.4	-661.2	6.2×1.9	91
M	8.65	1.49	1.26	<0.01	0.14	82.5	9.4	45.0	-149.9	-506.1	5.4×0.7	90
N	6.55	0.55	-0.61	0.045	<0.01	-112.8	8.5	8.0	-136.2	-526.8	14.2×3.2	176
O	5.95	2.46	-2.23	<0.01	0.17	-92.5	7.1	45.0	-149.7	-505.0	7.4×2.5	113

* Reference position: R.A.=20^h38^m36^s414±0⁰003 Dec.=42°37'35"44±0"03 (J2000)

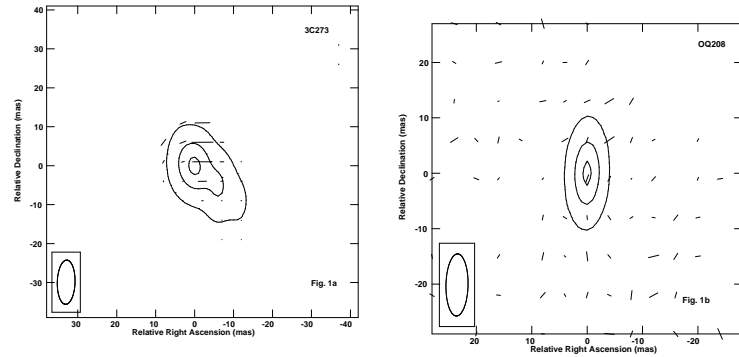


Fig. 1.— Continuum maps of calibration sources. a) 3C273. Contours - total intensity I: 0.9, 4.6, 8.3 Jy/beam; vectors - linearly polarized intensity, maximum length=0.125 Jy/beam; $m_L = 1.4\%$; $m_C = 1.8\%$ b) OQ208. Contours - total intensity I: 0.085, 0.45, 0.77 Jy/beam; vectors - linearly polarized intensity; 1 mas=0.0004 Jy/beam. $m_L \leq 0.8\%$; $m_C = 1.8\%$.

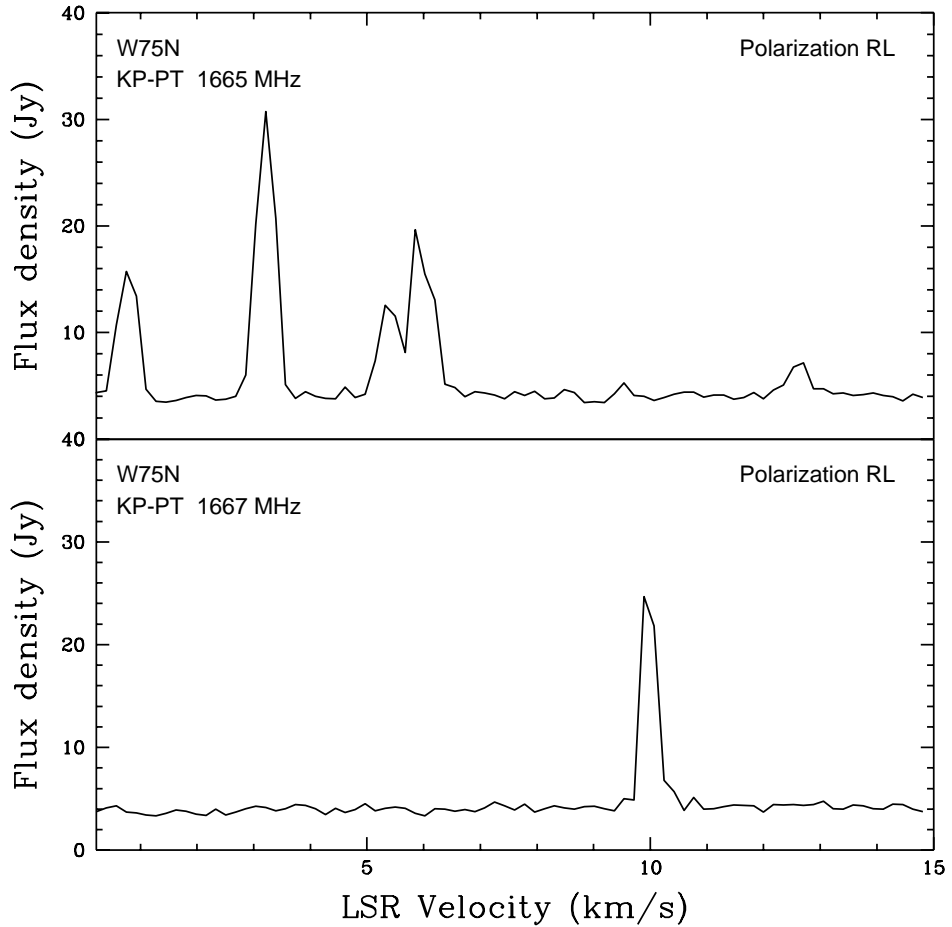


Fig. 2.— The cross power spectra of W75N on the base line Kitt Peak - Pie Town. Upper: cross-polarized RL spectrum of 1665 MHz OH line; lower: cross-polarized RL spectrum of 1667 MHz OH line.

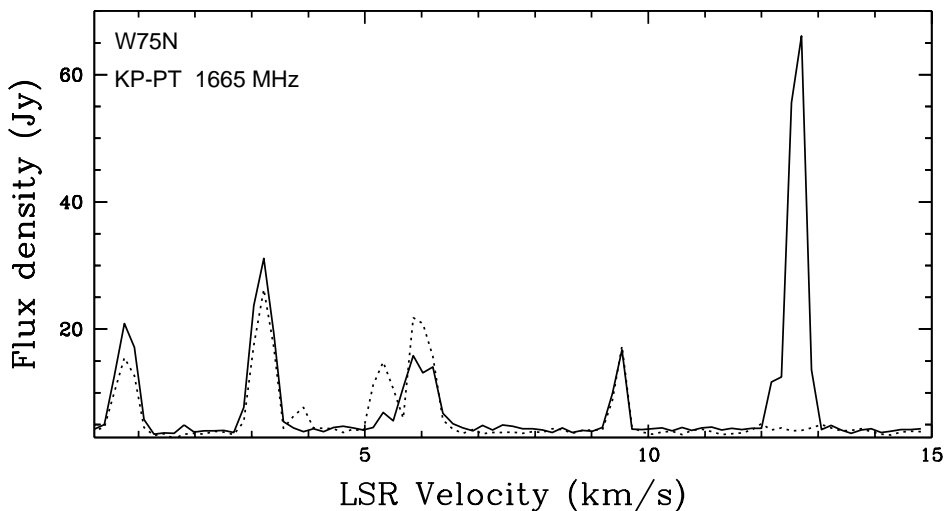


Fig. 3.— The cross power circularly polarized spectra of W75N on the base line Kitt Peak - Pie Town in 1665 MHz OH line. Dotted line: left-circular polarization (LCP); solid line: right-circular polarization (RCP).

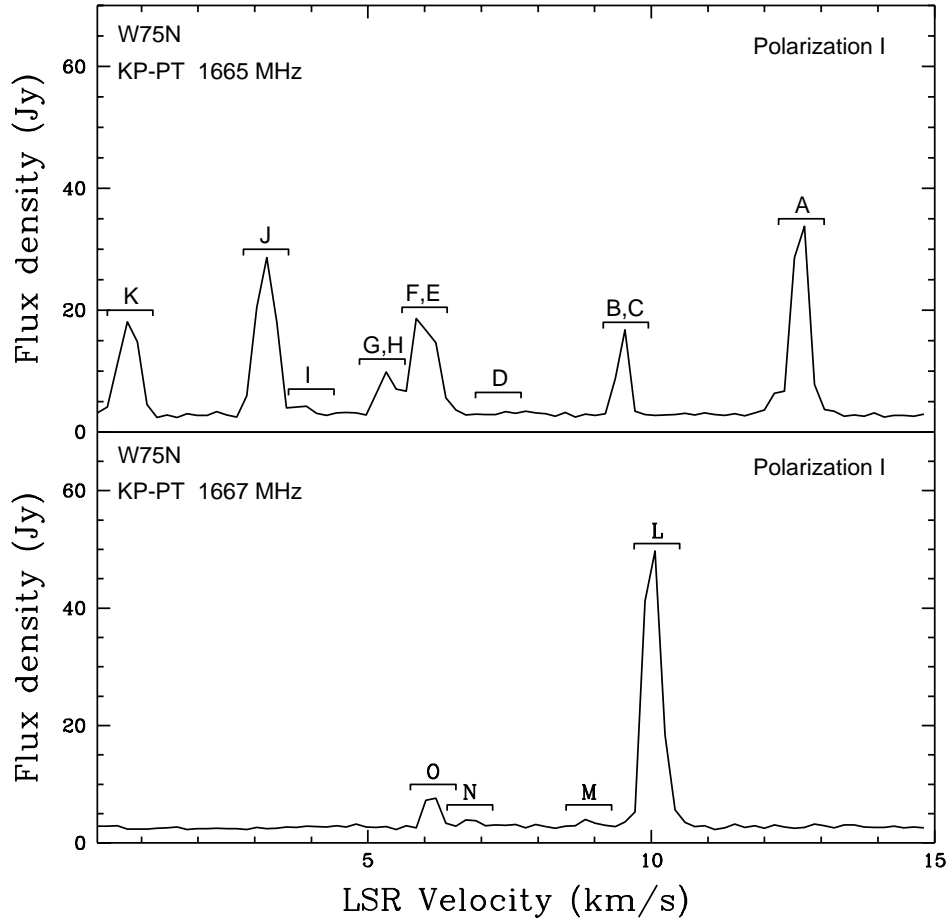


Fig. 4.— Total intensity I cross power spectra of W75N in 1665 MHz (upper) and 1667 MHz (lower) OH lines. Letters A - O mark spectral features which were mapped and their map and polarization parameters are given in Table 1.

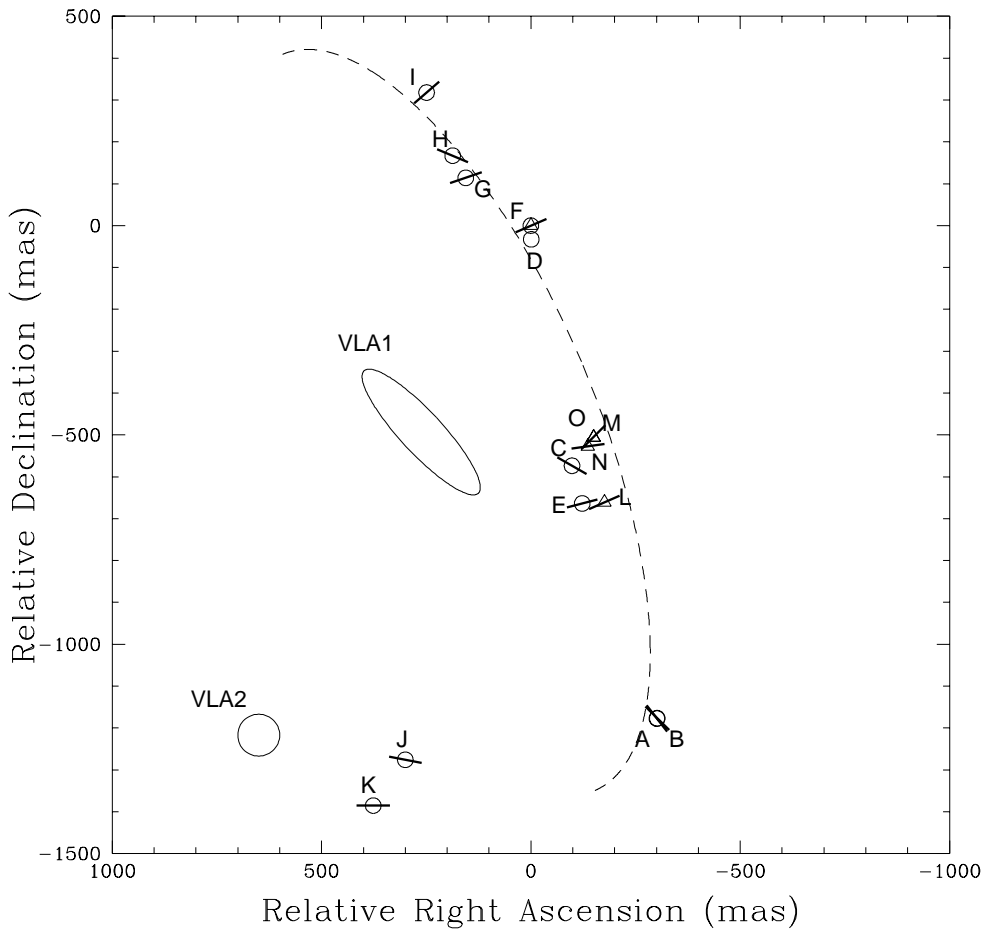


Fig. 5.— A VLBA map of the OH maser features. Circles denote 1665 MHz features, triangles - 1667 MHz features. They are labeled as in Table 1. Vectors attached to the maser features show relative direction of the magnetic field. An ellipse and a circle labelled VLA1 and VLA2 show position and size of ultra compact HII regions, from Torrelles et al (1997). Dashed line shows a portion of a possible disk centered at VLA1 and inclined by 12° to the line of sight.

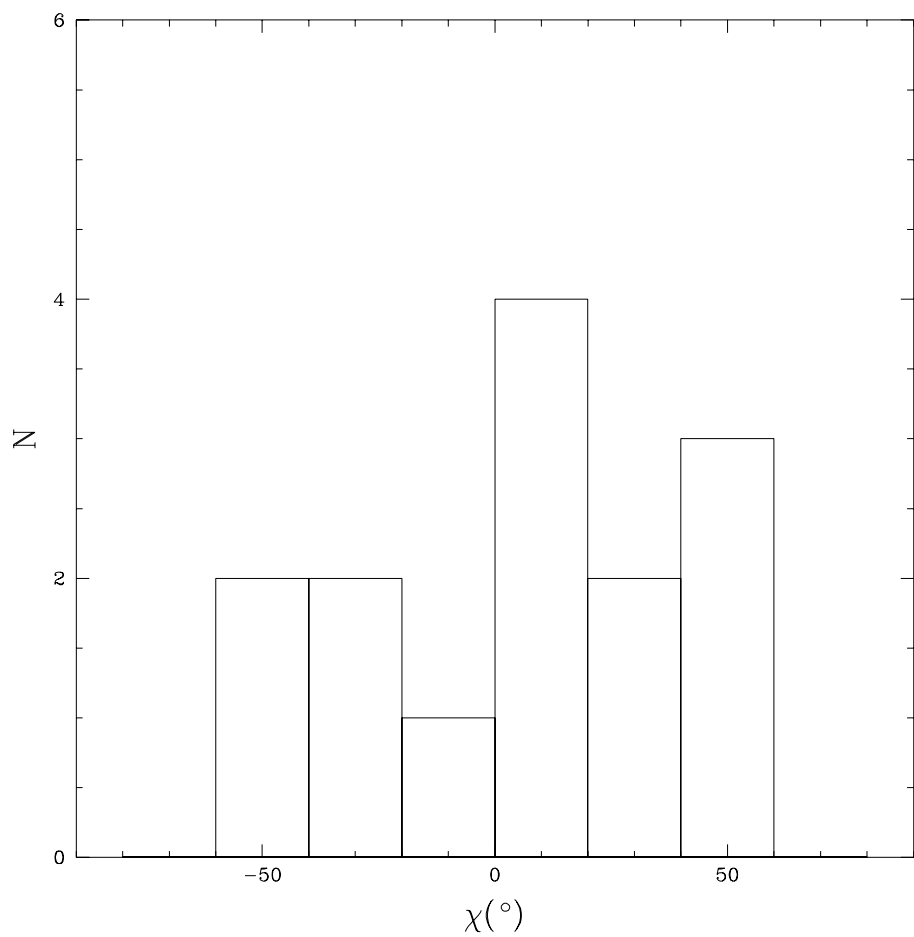


Fig. 6.— Distribution of the linear polarization relative position angles χ for maser spots in W75N. $\bar{\chi} = 4^\circ \pm 17^\circ$.

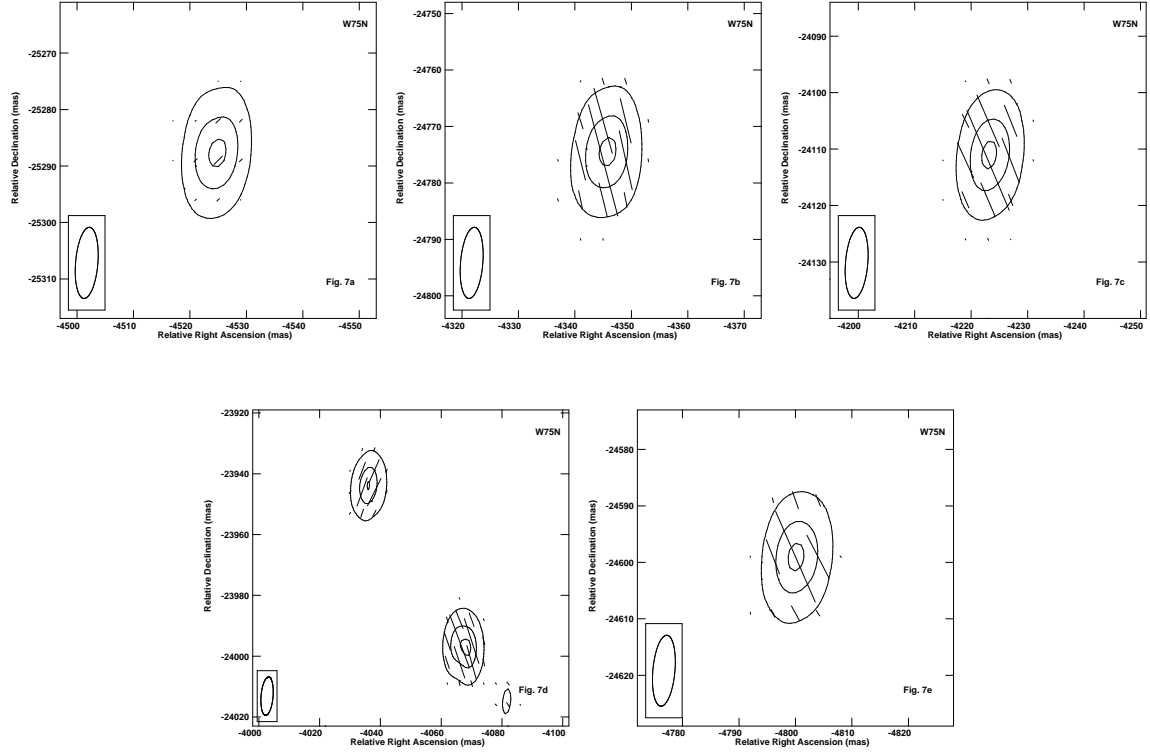


Fig. 7.— Linearly polarized and total intensity - maps of maser spots in W75N. a) Spot A: vector - linear polarization intensity (length) and relative position angle (direction); contours – total intensity: $0.1, 0.5, 0.9 \times (\text{peak intensity})$. Peak values $\sqrt{Q^2 + U^2} = 1.6$ Jy/beam, $I=16.9$ Jy/beam; b) Spot E: $\sqrt{Q^2 + U^2} = 5.4$ Jy/beam, $I=5.8$ Jy/beam; c) Spot F: $\sqrt{Q^2 + U^2} = 9.9$ Jy/beam, $I=10.2$ Jy/beam; d) Spots G and H: (G) $\sqrt{Q^2 + U^2} = 3.0$ Jy/beam, $I=3.3$ Jy/beam; (H) $\sqrt{Q^2 + U^2} = 2.0$ Jy/beam, $I=2.9$ Jy/beam; e) Spot L: $\sqrt{Q^2 + U^2} = 8.9$ Jy/beam, $I=21.3$ Jy/beam.

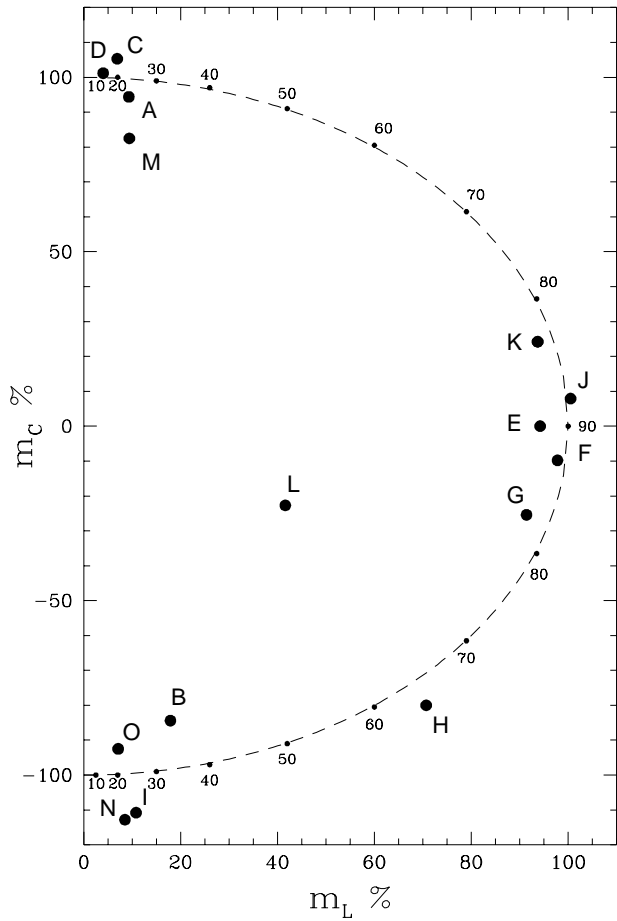


Fig. 8.— Percentage of circular polarization m_C of maser spots in W75N, plotted against percentage of linear polarization m_L . A completely polarized feature would lie on the dotted line. Negative values of m_C indicate LH circular or elliptical polarization and correspond to negative V in Table 1.

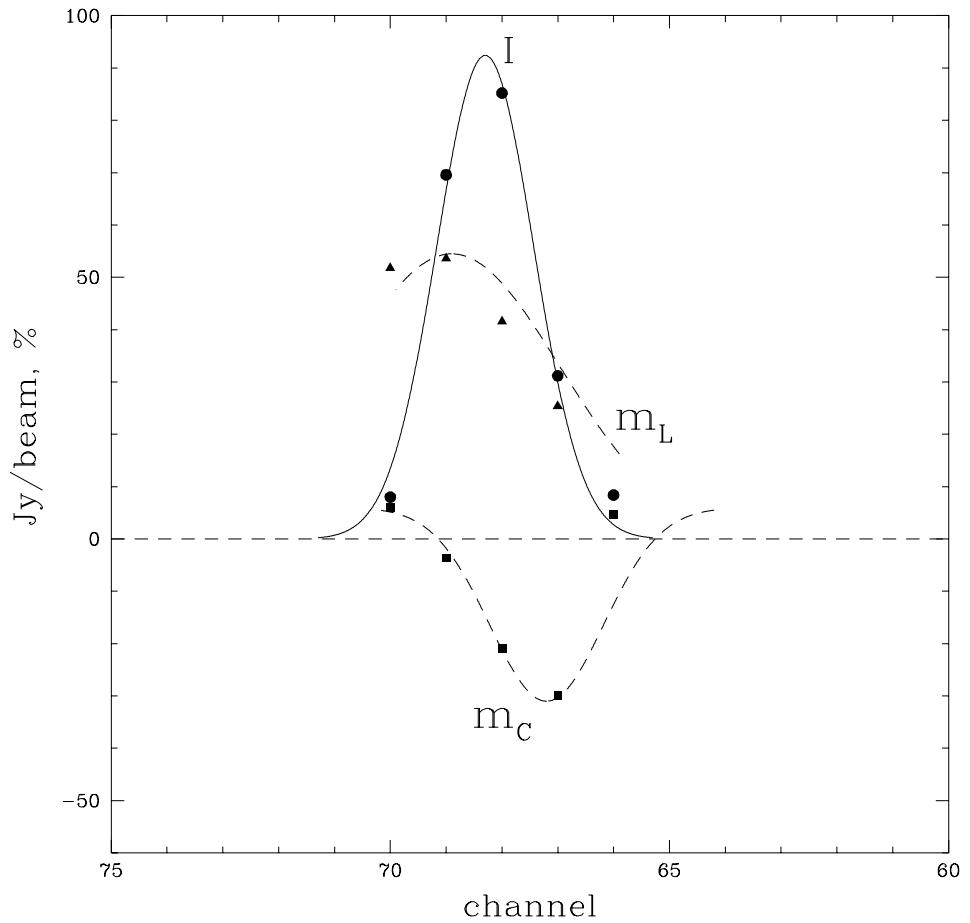


Fig. 9.— Line profile of 1667 MHz Spot L. Solid line (filled circles): total intensity I; dashed line (triangles): percentage of linear polarization m_L ; dashed line (squares): percentage of circular polarization m_C .